Journal of Environmental Engineering and Landscape Management
ISSN 1648–6897 / eISSN 1822-4199
2018 Volume 26 Issue 1: 38–56
https://doi.org/10.3846/16486897.2017.1346513

FIXED-BED COLUMN ADSORPTION OF ARSENIC(V) BY POROUS COMPOSITE OF MAGNETITE/HEMATITE/CARBON WITH EUCALYPTUS WOOD MICROSTRUCTURE

Yanhong LI[1, 2], Yinian ZHU[2*], Zongqiang ZHU[2], Xuehong ZHANG[2], Dunqiu WANG[2], Liwei XIE[2]

[1]*College of Light Industry and Food Engineering, Guangxi University, Nanning, Guangxi 530004, P.R. China*
[2]*College of Environmental Science and Engineering, Guilin University of Technology, Guilin, Guangxi 541004, P.R. China*

Received 15 January 2017; accepted 21 June 2017

Abstract. The fixed-bed column adsorption-desorption of As(V) by the porous composite of iron oxides and carbon with eucalyptus wood hierarchical microstructure (PC-Fe/C) was experimentally studied. The increase in the influent As(V) concentration and the inflow rate resulted in an earlier exhaustion of the column. The breakthrough curves indicated that a larger adsorbent mass, a smaller adsorbent grain size and a lower influent pH prolonged the column life span. The operating temperature had negligible effect. All breakthrough curves could be well fitted with the Thomas and Yoon–Nelson models. Under the condition of the influent flow rate of 5.136 mL/min, the influent As(V) concentration of 20 mg/L, the influent pH of 3, the adsorbent mass of 2 g, the adsorbent grain size of <100 mesh, and the operating temperature of 35 °C, the equilibrium adsorption capacity reached 10.49 mg/g, which was greater than those of natural/synthetic iron oxides adsorbents and iron-oxide-coated adsorbents.

Keywords: fixed-bed column adsorption, arsenic (V), biomorph-genetic adsorbent, iron oxide, carbon, eucalyptus wood microstructure.

Introduction

Arsenic contamination is the most serious worldwide human health threat due to its extremely toxic effects on animals and plants (Banerji, Chaudhari 2016; Smith *et al.* 2015). Arsenic, one of WHO's 10 chemicals of major public health concern, can be released into environment through many natural processes and various human activities (WHO 2016; Acosta *et al.* 2015; Mohan, Pittman 2007; Smedley, Kinniburg 2002). Long-term arsenic exposure can result in cancer in skin/lungs/urinary tracts, neurotoxicity, diabetes and cardiovascular disease (Sabbatini *et al.* 2010). The maximum arsenic limit of 10 μg/L in drinking water has been recommended by the World Health Organization (WHO) and acknowledged by many countries (WHO 2016).

Various treatment technologies, e.g. coagulation and precipitation, adsorption, membrane filtration, ion exchange, reverse osmosis and phytoremediation, have been developed for arsenic removal from drinking water and wastewater (Mishra, Mahato 2016). Among these available technologies, the adsorption is regarded as one of the most simple and effective methods (Sinha *et al.* 2011). In the past twenty years, lots of works have been done to investigate arsenate and arsenite adsorption by different adsorbents such as iron oxides and hydroxides, activated carbon, activated alumina and Al hydroxides, Fe/Mn oxide pillared clays, fly ash and graphene (Sinha *et al.* 2011; Yean *et al.* 2005). Iron (hydr)oxides available in different mineral forms, e.g. magnetite (Fe_3O_4), hematite (Fe_2O_3), goethite (α-FeOOH) and hydrous ferric oxide (HFO), have been proved to be suitable for As removal due to their low cost, high efficiency and little risk (Habuda-Stanić *et al.* 2008).

The specific surface area is a key parameter for adsorption. Thus, synthesis of iron oxides adsorbent with large surface area can increase the adsorption capacity for arsenic. Recently, nanomaterials have drawn an important attention because of their unique properties, e.g. large surface area, large number of active sites, small diffusion resistance and high reactivity (Lata, Samadder 2016). But

*Corresponding author. E-mail: *zhuyinian@glut.edu.cn*

Copyright © 2018 The Author(s). Published by VGTU Press

This is an Open Access article distributed under the terms of the Creative Commons Attribution License (http://creativecommons.org/licenses/by/4.0/), which permits unrestricted use, distribution, and reproduction in any medium, provided the original author and source are credited.

the magnetic separation of fine iron oxides nanoparticles from water is hard to carry out and very expensive. Moreover, for the <15nm nanoparticles, the separation could be ineffective and the residual particles in the effluent could cause some toxic problems. Additionally, their stability under different treatment conditions is uncertain (Mishra, Mahato 2016; Mohan, Pittman 2007). Therefore, developing the ideal adsorbents to remove contaminants through fixed-bed column adsorption is still a goal of many researchers (Habuda-Stanić *et al*. 2008).

The hierarchical porous microstructure of plants ranges from the millimeter-scale (growth ring pattern of wood) to the micrometer-scale (cellulose fiber structures) (Sieber 2005). Great efforts had been made to convert these microstructures into microcellular designed materials in manufacturing adsorbents, which hold the hierarchical porous microstructure like a negative duplication of the plant biotemplates (Zhu *et al.* 2015). The hierarchical porous adsorbent is advantageous in the application needing interconnected porosities, e.g. filtering (Presas *et al.* 2006).

The porous composite of $Fe_3O_4/Fe_2O_3/C$ (PC-Fe/C) has been developed by using eucalyptus wood as microstructural biotemplate and confirmed to be effective for As(V) adsorption through batch experiments (Wei *et al.* 2013). However, the adsorption parameters obtained from batch experiments are generally not suitable for column operations. Thus, it is still needed to do equilibrium tests by using fixed-bed columns (Han *et al.* 2007). The main purpose of this work is to study the effectiveness of the PC-Fe/C application for the column adsorption of As(V) from aqueous solution. The effects of influent initial concentration, inflow rate, influent pH, adsorbent mass, adsorbent grain size and operating temperature on arsenic(V) adsorption by the PC-Fe/C-packed column were investigated. The Thomas, Yoon–Nelson, Adams–Bohart, Wolborska and Clark models were used to fit the performances.

1. Materials and methods

1.1. Adsorbent preparation and characterization

1.1.1. Preparation

In order to increase the connectivity among pores and cellular of the biotemplates efficiently, the biotemplates of *Eucalyptus* wood chips (30×10×3 mm^3) were first boiled in 5% ammonia solution for 6h to extract gums, tropolones, fats, fatty acid, and so on. The biotemplates were then rinsed in ultrapure water and dried at 80 °C for 24 h. After the extraction treatment, they were soaked in a precursor solution of 1.2 mol/L $Fe(NO_3)_3$ in a binary (1:1) ethanol/water solvent at 60 °C for 3d and then dried at 80 °C for 1d. This soaking-drying process was repeated 3 times. Finally, the soaked-dried biotemplates were heated in a muffle furnace slowly to 600 °C at 4 °C/min and kept at 600 °C for 3h. After cooling to room temperature, the porous composites of $Fe_3O_4/Fe_2O_3/C$ (PC-Fe/C) with eucalyptus wood hierarchical microstructure were obtained.

1.1.2. Characterization

The chemical component of the $Fe_3O_4/Fe_2O_3/C$ adsorbent (PC-Fe/C) prepared was determined using an Element Analyzer (EA2400II, PerkinElmer). A Quantachrome NOVAe1000 was used to measure the BET (Brunauer-Emmett-Teller) specific surface area. The adsorbent was also analyzed using an X'Pert PRO X-ray diffractometer (PANalytical B.V.) and identified by comparing with the ICDD (International Center for Diffraction Data) standards. The FT-IR spectra were recorded from 4000 to 400 cm^{-1} in a form of KBr pellets by a Nicolet Nexus 470 FT-IR spectrophotometer (Thermo Fisher Scientific Inc.). Furthermore, the adsorbent morphology was examined using a Jeol JSM-6380LV scanning electron microscopy (Japan Electron Optics Ltd.).

1.2. Column experiments

1.2.1. Adsorption

The columns with an inner diameter of 12.8 mm and a length of 140 mm were used for the rapid small-scale column test (RSSCT). Plastic meshes and fiber glass were put on the column bottom and top to support the adsorbent to avoid the adsorbent loss and keep the adsorbent density in adsorption. A certain amount of the PC-Fe/C adsorbent was packed into each column and wetted with pure water in downward flow direction to withdraw the air trapped among particles. Stock arsenate solutions were prepared with analytical grade sodium arsenate ($Na_3AsO_4{\cdot}12H_2O$) and nitric acid (HNO_3). A BL100-DG peristaltic pump (Changzhou PreFluid Technology Co., Ltd., China) was used to feed the As(V) working solution continuously downward into the column. The effluents were sampled at the time interval of 20 min, filtered through a 0.22 μm microporous membrane, acidified with nitric acid solution and preserved at 4 °C until analyses. The residual As(V) concentrations were measured using a SA-20 atomic fluorescence spectrometry (Beijing Titan Instruments Co., Ltd., China).

The effects of influent flow rate, initial As(V) concentration, influent pH, adsorbent mass, adsorbent grain size and operating temperature on adsorption removal capacity were investigated. The As(V) stock solution was diluted to 10, 20, 30 and 50 mg/L and the influent pH was adjusted to 1~10 to determine the As(V) adsorption capability of PC-Fe/C. The influent flow rate was adjusted to 3.434, 5.136, 10.27 and 15.41 mL/min to examine the influence of inflow rate. To value the effect of adsorbent mass, the PC-Fe/C of different amounts (1, 2, 3, and 4 g or 0.85 cm, 1.69 cm, 2.54 cm and 3.38 cm in bed depth) were packed in four separate columns. The PC-Fe/C adsorbents of 20~40 mesh (0.841~0.4 mm), 40~60 mesh (0.4~0.25 mm), 60~80 mesh (0.25~0.177 mm), 80~100 mesh (0.177~0.149 mm) or <100 mesh (<0.149 mm) were chosen to investigate the effect of adsorbent grain size. 25 °C, 35 °C or 45 °C were used to study the effect of temperature.

1.2.2. Desorption

0.50 g of the PC-Fe/C adsorbent (<100 mesh) was first agitated (150 rpm) with 50 mL of 20 mg/L As(V) solution of pH 8 by a thermostatic water bath oscillator for 1 h at 35 °C. And then, the As(V)-saturated adsorbent was taken out and agitated in 50 mL of 0.1 mol/L desorption solvent (NaOH, $NaHCO_3$, NaCl or H_2O) at 150 rpm and room temperature for 1 h. After that, the optimal desorption solvent was chosen for further column investigation. Three adsorption–desorption cycles were made in a continuous fixed-bed column. The As(V) working solution was first continuously fed downward into the column by a peristaltic pump. The influent initial concentration, the influent flow rate, the influent, the adsorbent mass, the adsorbent grain size and temperature were controlled at 20 mg/L, Q = 5.136 mL/min, pH = 3, m = 2g, <100 mesh and T = 35 °C, respectively. At the time interval of 20min, the effluent was collected, filtered and analyzed. When the effluent reached the exhaustion point (the exhaustion concentration = 18 mg/L), the feeding of the As(V) working solution was stopped. Then, 0.1 mol/L NaOH solution as desorption solvent was continuously fed upward into the column by a peristaltic pump. At the time interval of 20 min, the effluent was also collected, filtered and analyzed. The effect of desorption solvent concentration, influent rate and temperature was studied.

1.3. Mathematical description of fixed-bed column studies

The total adsorbed As(V) (q_{total}) by the column can be calculated by integrating the plot of the adsorbed As(V) concentration ($C_{ad} = C_0 - C_t$) against the flow time (t). The area (A) under this integrated plot is substituted in Eq. (1) to determine q_{total}:

$$q_{total}\,(\text{mg}) = \frac{QA}{1000} = \frac{Q}{1000}\int_{t=0}^{t=t_{total}} C_{ad}\,dt. \quad (1)$$

The total amount of As(V) flowing through the column (m_{total}) can be calculated with Eq. (2):

$$m_{total}\,(\text{mg}) = \frac{C_0 Q t_{total}}{1000}, \quad (2)$$

where, the t_{total} and Q represent the total flow time (min) and the volumetric inflow rate (mL/min), respectively.

The total removal efficiency of As(V) can be used to evaluate the column performance, as expressed in Eq. (3):

$$\text{Total removal efficiency } (Y) = \frac{q_{total}}{m_{total}} \times 100\,. \quad (3)$$

The column maximum adsorption capacity, also known as the equilibrium metal ion uptake (q_e), is calculated using Eq. (4):

$$q_e\,(\text{mg/g}) = \frac{q_{total}}{x}, \quad (4)$$

in which, x is the unit mass of adsorbent packed in the column.

1.4. Adsorption modeling for fixed bed column studies

Generally, the breakthrough curve of the continuous fixed bed system can be expressed as C_t/C_0 versus the flow time (t), in which C_0 and C_t represent the influent and effluent As(V) concentrations, respectively (Han *et al.* 2007; Goel *et al.* 2005). The application of the column adsorption kinetic models is essential to provide further description of the column performance or to evaluate the strengths and weaknesses for the current adsorbent and column design. The column parameters show the most important effects on the column performance and optimum operation factors that contributed to the effective removal of As(V) ions. Hence, suitable parameters are important for the column operation to achieve optimum performance. Additionally, the theoretical models can be applied to the experimental data to further describe the adsorption mechanism. Because the adsorption process is not at a steady state as the influent flows through the fixed-bed column under predesigned operating conditions, it is not easy to express the dynamic behavior of adsorbate in the column. However, the modeling of data has been made in this work using the mathematical models such as the Thomas, Yoon–Nelson, Adams–Bohart, Wolborska and Clark models, which were constructed to describe and predict the dynamic behavior of the break through curves and have been used by various authors (Ghosh *et al.* 2014). The theoretical predicted points (lines) with the five models were superposed on the breakthrough curves of the experimental results (points).

The Thomas model is among the models commonly selected to conduct prediction of the breakthrough results (Lim, Aris 2014). The Thomas model has the following linearized form:

$$\ln\left[\frac{C_0}{C_t} - 1\right] = \frac{k_{Th} q_e m}{Q} - k_{Th} C_0 t\,, \quad (5)$$

where k_{Th} is the Thomas rate constant (mL/min·mg) and q_e is the column maximum adsorption capacity (mg/g), which can be determined from a plot of $\ln[(C_0/C_t]-1]$ against t at a given flow rate.

The Yoon–Nelson model is known to be a simple theoretical model because less column data is needed to construct the model, and it is suitable for the single component system (Lim, Aris 2014). The linearized equation can be described as:

$$\ln\left[\frac{C_t}{C_0 - C_t}\right] = k_{YN} t - \tau k_{YN}\,, \quad (6)$$

in which, k_{YN} is the rate constant (1/min) and τ is the time required for 50% adsorbate breakthrough (min), which can be obtained from the plot of $\ln[C_t/(C_0 - C_t)]$ *versus* t. The linearized Yoon–Nelson equation is similar to the linearized form of the Thomas model.

The Clark model combines the mass transfer concept with the Freundlich equation:

$$\ln\left[\left(\frac{C_t}{C_o}\right)^{1-n} - 1\right] = \ln A - rt, \quad (7)$$

where n is the Freundlich constant, A is the constant of the Clark model (min) and r is the adsorption rate (mg/L·min).

The Adams–Bohart model is usually selected for the prediction of the breakthrough for the initial part of the adsorption process. The model can be described as Eq. (8):

$$\ln\left[\frac{C_t}{C_0}\right] = k_{AB}C_0 t - k_{AB}N_0\frac{Z}{U_0}, \quad (8)$$

where the k_{AB} represents the Adams–Bohart kinetic constant (L/mg min). The Z and N_0 are the bed depth of column (cm) and the saturation concentration (mg/L), respectively. The U_0 is the linear velocity (cm/min) determined from the calculation of volumetric flow rate over the bed section area.

The Wolborska model can also be used to describe the breakthrough for the initial part of the adsorption dynamics with Eq. (9):

$$\ln\left[\frac{C_t}{C_0}\right] = \frac{\beta_a C_0}{N_0}t - \frac{\beta_a Z}{U_0}, \quad (9)$$

where β_a is the kinetic coefficient of the external mass transfer (1/min). The Wolborska expression is the same as the Adams–Bohart equation when $k_{AB} = \beta_a/N_0$.

2. Results and discussion

2.1. Characterization of the adsorbent

The Fe, O, C and H contents of the PC-Fe/C adsorbent were 62.51~65.37%, 20.46~20.52%, 10.73~10.96% and 3.04~5.52%, respectively. The BET surface area of PC-Fe/C was 59.2 m^2/g, which was comparable to those for natural or synthetic iron oxides (Zhu *et al.* 2015) and decreased to 29.9 m^2/g after As(V) adsorption. The XRD analysis showed that the PC-Fe/C adsorbent was composed of magnetite (Fe_3O_4), hematite (α-Fe_2O_3) and carbon (Figure 1). Additionally, the PC-Fe/C adsorbent has a point of zero charge at pH_{PZC} of 3.2. In the FT-IR spectra of the adsorbent after sorption of As(V), the peaks of AsO_4^{3-} tetrahedra for the O-As-O bending around 424.26 cm^{-1} (ν_4), 447.40~466.69 cm^{-1} (ν_4) and 634.47~692.32 cm^{-1} (ν_2) were observed, and the peaks of AsO_4^{3-} tetrahedra for the As-O stretching appeared around 860.10~877.45 cm^{-1} (ν_3) (Figure 2).

The PC-Fe/C adsorbent maintained the hierarchical porous microstructure of eucalyptus wood very well (Figure 3). Pores of three different sizes, i.e., macropores (widths 70~120 μm) originated from vessels, mesopores (widths 4.1~6.4 μm) from fiber pores and micropores (widths 0.1~1.3 μm) from pits on the walls of the fiber pores and vessels, were retained from eucalyptus wood (Figure 3). The extracting pre-treatment procedure could greatly increase the interpore connectivity.

2.2. Column adsorption

2.2.1. Effect of influent concentration

The equilibrium uptake of As(V) oxyanions increased with the increase of the influent As(V) concentrations from 10 mg/L to 50 mg/L (Figure 4, Table 1). The unadsorbed As(V) concentrations at the equilibrium increased also along with the higher influent concentrations. This showed that the bed saturated quicker when a large amount of As(V) oxyanions were introduced to the adsorbent column. In the As(V) breakthrough curves, all four influent As(V) concentrations exhausted within 580 minutes. The PC-Fe/C is possibly favorable for As(V)

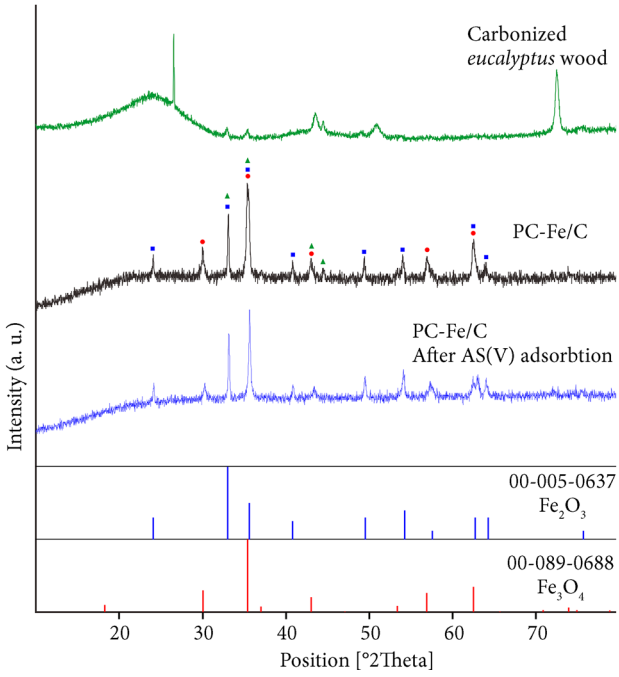

Figure 1. XRD patterns of the PC-Fe/C adsorbent prepared with eucalyptus wood biotemplate

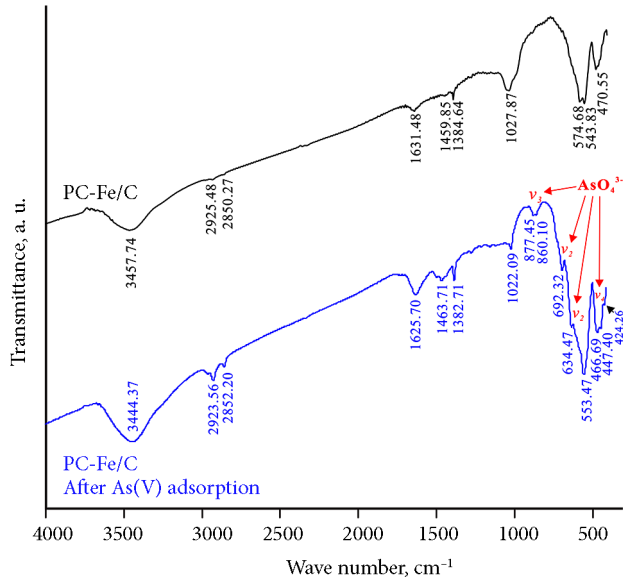

Figure 2. FT-IR spectra of the PC-Fe/C adsorbent prepared with eucalyptus wood biotemplate

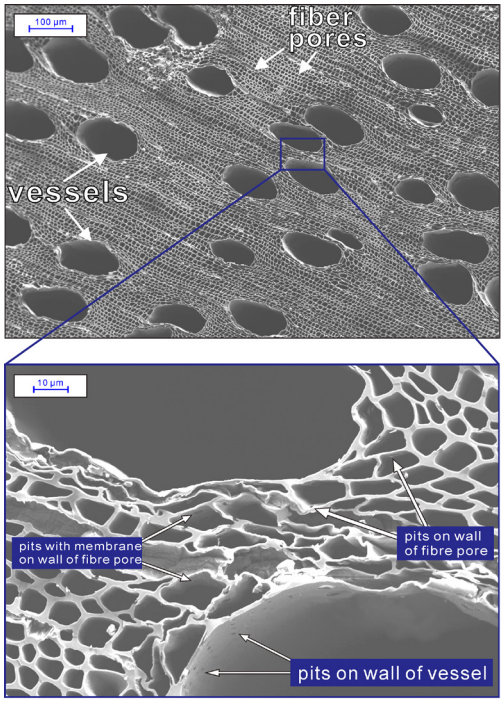

Figure 3. SEM result of the PC-Fe/C adsorbent prepared with eucalyptus wood biotemplate

adsorption. With the higher load of As(V) oxyanions, the column performance was fast in the beginning and remained constant at equilibrium after the removal efficiency began to decrease.

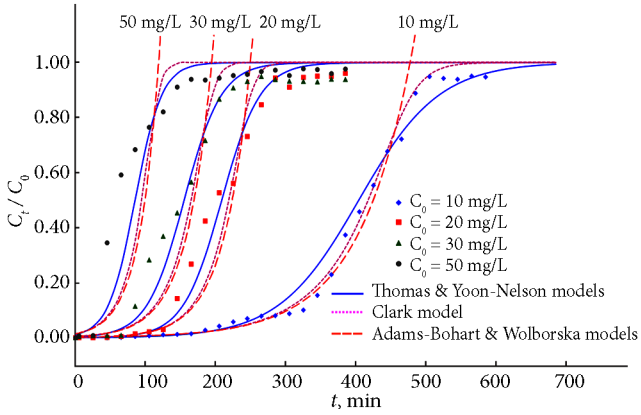

Figure 4. Effect of influent concentration on breakthrough curve for As(V) adsorption removal by the PC-Fe/C adsorbent prepared with eucalyptus wood template (flow rate: 5.136 mL/min; pH: 3; adsorbent mass: 2 g; adsorbent grain size: <100 mesh; operating temperature: 35 °C)

Table 1. Parameters of the Thomas model using linear regression analysis and the equilibrium As(V) uptake (q_e) and the total removal percentage (Y) for As(V) sorption to PC-Fe/C under different conditions

Influent concentr. C_0, mg/L	Flow rate Q, mL/min	Sorbent mass x, g	Sorbent grain size, mesh	Operating temp. T, °C	Influent pH	k_{Th}, mL/min mg	$q_{e,calc}$, mg/g	$q_{e,exp}$, mg/g	Y, %	R^2
10	5.136	2	<100	35	3	0.00175	10.38	10.34	79.70	0.9642
20	5.136	2	<100	35	3	0.00183	10.72	10.49	71.63	0.9807
30	5.136	2	<100	35	3	0.00126	11.95	11.41	65.80	0.9507
50	5.136	2	<100	35	3	0.00106	10.93	9.19	49.35	0.8367
20	3.434	2	<100	35	3	0.00111	12.67	12.63	79.09	0.9807
20	5.136	2	<100	35	3	0.00183	10.72	10.49	71.63	0.9807
20	10.27	2	<100	35	3	0.00207	15.64	14.99	64.87	0.9719
20	15.41	2	<100	35	3	0.00277	12.86	13.01	67.56	0.9399
20	5.136	1	<100	35	3	0.00168	11.73	10.34	49.08	0.8776
20	5.136	2	<100	35	3	0.00183	10.72	10.49	71.63	0.9807
20	5.136	3	<100	35	3	0.00197	10.88	9.31	61.11	0.8599
20	5.136	4	<100	35	3	0.00172	11.70	11.25	74.88	0.9017
20	5.136	2	20–40	35	3	0.00202	5.01	4.51	53.20	0.8944
20	5.136	2	40–60	35	3	0.00222	6.45	6.11	64.32	0.9466
20	5.136	2	60–80	35	3	0.00193	7.98	6.60	57.07	0.9636
20	5.136	2	80–100	35	3	0.00139	8.03	7.57	55.60	0.8974
20	5.136	2	<100	35	3	0.00183	10.72	10.49	71.63	0.9807
20	5.136	2	<100	25	3	0.00205	9.56	9.16	67.30	0.9488
20	5.136	2	<100	35	3	0.00183	10.72	10.49	71.63	0.9807
20	5.136	2	<100	45	3	0.00185	11.28	11.01	75.21	0.9856
20	5.136	2	<100	35	1	0.00163	9.90	8.30	67.62	0.9790

End of Table 1

Influent concentr. C_0, mg/L	Flow rate Q, mL/min	Sorbent mass x, g	Sorbent grain size, mesh	Operating temp. T, °C	Influent pH	k_{Th}, mL/min mg	$q_{e,calc}$, mg/g	$q_{e,exp}$, mg/g	Y, %	R^2
20	5.136	2	<100	35	2	0.00197	9.78	9.46	69.50	0.9859
20	5.136	2	<100	35	3	0.00183	10.72	10.49	71.63	0.9807
20	5.136	2	<100	35	4	0.00229	7.05	6.81	64.67	0.9901
20	5.136	2	<100	35	5	0.00219	6.29	6.26	65.86	0.9907
20	5.136	2	<100	35	6	0.00217	6.04	5.74	60.36	0.9672
20	5.136	2	<100	35	7	0.00253	4.27	3.92	52.59	0.9524
20	5.136	2	<100	35	8	0.00238	3.08	2.78	43.37	0.9060
20	5.136	2	<100	35	9	0.00157	1.34	1.92	35.59	0.9637
20	5.136	2	<100	35	10	0.00175	1.82	2.17	40.24	0.9668

Note: the subscripts "exp" and "calc" show the experimental and calculated values.

The breakthrough occurred gradually and the breakthrough curves scattered at lower influent As(V) concentrations. The sharper breakthrough curve occurred when the influent As(V) concentration increased (Figure 4). The breakthrough (C_t = 0.5 mg/L) at the influent As(V) concentration of 50mg/L appeared after 26 min (133.54 mL of effluent solution) while the breakpoint time (C_t = 0.5 mg/L) at the influent As(V) concentration of 10 mg/L occurred after 216 min (1109.38 mL of effluent solution) (Table 2). The breakthrough time increased

Table 2. Parameters of the Yoon–Nelson model using linear regression analysis for As(V) sorption to PC-Fe/C under different conditions

Influent concentr. C_0, mg/L	Flow rate Q, mL/min	Sorbent mass x, g	Sorbent grain size, mesh	Operating temp. T, °C	Influent pH	k_{YN}, min^{-1}	τ_{calc}, min	τ_{exp}, min	$\Delta\tau/\tau_{exp}$, %	$t_{1,\,calc}$, min	$t_{1,\,exp}$, min	$t_{2,\,calc}$, min	$t_{2,\,exp}$, min	R^2
10	5.136	2	<100	35	3	0.0175	404	414	2.37	236	216	530	489	0.9642
20	5.136	2	<100	35	3	0.0365	209	200	4.34	108	114	269	277	0.9807
30	5.136	2	<100	35	3	0.0378	155	179	13.33	47	67	213	222	0.9507
50	5.136	2	<100	35	3	0.0528	85	58	46.72	–	26	127	143	0.8367
20	3.434	2	<100	35	3	0.0222	369	391	5.62	204	199	468	461	0.9807
20	5.136	2	<100	35	3	0.0365	209	200	4.34	108	114	269	277	0.9807
20	10.27	2	<100	35	3	0.0414	152	137	11.13	64	75	205	214	0.9719
20	15.41	2	<100	35	3	0.0554	83	88	5.14	17	4	123	120	0.9399
20	5.136	1	<100	35	3	0.0336	114	87	31.31	5	27	180	203	0.8776
20	5.136	2	<100	35	3	0.0365	209	200	4.34	108	114	269	277	0.9807
20	5.136	3	<100	35	3	0.0393	318	237	34.11	225	187	374	436	0.8599
20	5.136	4	<100	35	3	0.0343	456	417	9.26	349	310	520	571	0.9017
20	5.136	2	20–40	35	3	0.0404	98	80	21.95	7	26	152	165	0.8944
20	5.136	2	40–60	35	3	0.0443	126	114	10.14	43	47	175	185	0.9466
20	5.136	2	60–80	35	3	0.0385	155	142	9.47	60	68	213	224	0.9636
20	5.136	2	80–100	35	3	0.0278	156	130	20.22	24	66	235	253	0.8974
20	5.136	2	<100	35	3	0.0365	209	200	4.34	108	114	269	277	0.9807
20	5.136	2	<100	25	3	0.0409	186	180	3.36	96	100	240	256	0.9488
20	5.136	2	<100	35	3	0.0365	209	200	4.34	108	114	269	277	0.9807
20	5.136	2	<100	45	3	0.0369	220	208	5.57	120	138	279	285	0.9856
20	5.136	2	<100	35	1	0.0325	199	195	1.90	86	90	266	277	0.9790

End of Table 2

Influent concentr. C_0, mg/L	Flow rate Q, mL/min	Sorbent mass x, g	Sorbent grain size, mesh	Operating temp. T, °C	Influent pH	k_{YN}, min^{-1}	τ_{calc}, min	τ_{exp}, min	$\Delta\tau/\tau_{exp}$, %	$t_{1,\,calc}$, min	$t_{1,\,exp}$, min	$t_{2,\,calc}$, min	$t_{2,\,exp}$, min	R^2
20	5.136	2	<100	35	2	0.0394	190	181	5.22	97	97	246	265	0.9859
20	5.136	2	<100	35	3	0.0365	209	200	4.34	108	114	269	277	0.9807
20	5.136	2	<100	35	4	0.0458	137	131	4.77	57	67	185	192	0.9901
20	5.136	2	<100	35	5	0.0437	122	128	4.34	39	47	173	174	0.9907
20	5.136	2	<100	35	6	0.0434	118	104	13.08	33	48	168	178	0.9672
20	5.136	2	<100	35	7	0.0505	83	71	17.14	11	26	127	134	0.9524
20	5.136	2	<100	35	8	0.0476	60	50	19.91	–	6	106	112	0.9060
20	5.136	2	<100	35	9	0.0313	26	29	9.76	–	–	96	95	0.9637
20	5.136	2	<100	35	10	0.0350	35	38	6.64	–	–	98	96	0.9668

Note: the subscripts "exp" and "calc" show the experimental and calculated values.

with the decreasing influent As(V) concentration since the adsorption sites in the fixed-bed became more slowly saturated. A increased influent As(V) concentration resulted in an early breakpoint time, and the treated volume was the smallest at the highest influent As(V) concentration because the higher concentration gradient could cause a quicker transport as a result of an increased diffusion coefficient or increased mass transfer coefficient, i.e., the difference between the As(V) concentration in the solution and the As(V) concentration on the adsorbent is the driving force for adsorption (Nwabanne, Igbok 2012). A greater concentration difference gives a larger driving force for adsorption and causes a larger adsorption capacity of the column fed. Moreover, the availability of the As(V) oxyanions for the adsorption sites was more at the higher influent As(V) concentration.

The equilibrium As(V) uptake (q_e) and the total As(V) removal efficiency (Y) are also showed in Table 1. The equilibrium adsorption capacities ($q_{e,exp}$) were 10.34 mg/g, 10.49 mg/g, 11.41 mg/g and 9.19 mg/g for the influent As(V) concentrations of 10 mg/L, 20 mg/L, 30 mg/L and 50 mg/L, respectively. The total As(V) removal efficiencies decreased from 79.70% to 49.35% with the increasing influent As(V) concentration from 10 to 50 mg/L. This indicated that the equilibrium As(V) uptake ($q_{e,exp}$) increased from 10.34 mg/g to 11.41 mg/g with the increasing influent As(V) concentration from 10 to 30 mg/L. However, a further increase of the influent As(V) concentration from 30 mg/L to 50 mg/L decreased the adsorption capacity. With respect to a lower influent As(V) concentration, the inflow adsorbate molecules were adequate to the active sites on the surface of the adsorbent. For a higher influent As(V) concentration, extreme inflow of As(V) (>30 mg/L) exceeded the limited available active sites on the adsorbent surface. Nevertheless, an increase in the influent As(V) concentration enhances the concentration gradient which can overcome mass transfer resistance and increase the adsorption capacity (Auta *et al.* 2013; Chen *et al.* 2011). The bed can been saturated faster when a larger amount of As(V) was introduced into the column reactor (Podder, Majumder 2016; Han *et al.* 2007; Goel *et al.* 2005).

2.2.2. Effect of influent flow rate

The influent flow rate of metal solution into the column is one of the most important parameters that affect the removal capacity of the bed column (Podder, Majumder 2016; Lim, Aris 2014). An increase in the influent flow rate into the adsorption column was synonymous with an increase in mass flow (Auta *et al.* 2013). The influent flow rates (Q) were varied to 3.434, 5.136, 10.27 and 15.41 mL/min for the column. The adsorption data versus flow rate are plotted in Figure 5, and the equilibrium As(V) uptake (q_e) and the total As(V) removal efficiency (Y) are showed in Table 1 and 2.

For the lowest flow rate of 3.434 mL/min applied in the columns system, the breakthrough curve in the column (C_t/C_0) was found to have a gradual curve than the 5.136, 10.27 and 15.41 mL/min. While for the highest flow rate of 15.41 mL/min, the breakthrough curve (C_t/C_0) of As(V) was seen to increase drastically at the initial part of the performance (Figure 5). The influent flow rate considerably affected the contact time between the adsorbate and adsorbent, which was comparatively longer with the decreased flow rate. Therefore, at the beginning of operation, the adsorption was incomplete and led to steep breakthrough result (Podder, Majumder 2016; Lim, Aris 2014). At the equilibrium, the un-adsorbed As(V) concentration increased as the inflow rate increased. As showed in Figure 5 and Table 1, at the lowest flow rate of 3.434 mL/min, most of As(V) was adsorbed at the operation beginning.

As the operation processed, the effluent As(V) concentration was rapidly close to the influent As(V) concentration and the PC-Fe/C bed in the column became saturated with As(V). The breakpoint time decreased with increasing flow rate. Much sharper breakthrough curves were observed at a higher flow rates. At the slowest inflow rate of 3.434 mL/min, the breakthrough time was longer as compared to the higher flow rate of 15.41 mL/min. Earlier saturation of the adsorbent bed was associated with the higher mass transfer coefficient due to the higher inflow rate. Therefore, a lower inflow rate would enhance the As(V) adsorption on the PC-Fe/C bed and slower the breakthrough, i.e., a decrease in the inflow rate would considerably increase the breakthrough time for saturation (Figure 5, Table 2).

Although a longer residence time at a lower inflow rate provided a longer time for diffusion of As(V) ions, the maximum adsorption capacity (q_e) of the column decreased with the decrease in the total amount of inlet As(V) i.e., the total influent volume at the exhausting point of $C_t/C_0 = 0.9$. The experimental q_e values were 12.63, 10.49, 14.99 and 13.01 mg/g for the inflow rates of 3.434, 5.136, 10.27 and 15.41 mL/min, respectively. The total As(V) influent volumes at the exhausting point of $C_t/C_0 = 0.9$ were 1583.07, 1422.67, 2197.78 and 1849.20 mL, and the total amounts of inlet As(V) were 31.66, 28.45, 43.96 and 36.98 mg for the inflow rates of 3.434, 5.136, 10.27 and 15.41 mL/min, respectively.

Figure 5 and Table 1 showed also that the removal efficiency was higher at a lower inflow rate. As(V) had a longer time in contact with adsorbent at a low inflow rate, which resulted in a higher removal of As(V) oxyanions in the PC-Fe/C column. The total adsorbed As(V) quantities also decreased from 79.09% to 67.56% with the increasing inflow rates from 3.434 mL/min to 15.41 mL/min. At the same time, the breakthrough curves became steeper and the column operation reached the breakthrough points quickly. This is because the contact time between the adsorbate and the adsorbent decreased and the rate of mass transfer increased at a higher inflow rate, i.e. the amount of As(V) adsorbed onto the unit bed depth (mass transfer zone) increased with the increase in inflow rate resulting in faster saturation and early breakthrough (Nwabanne, Igbokw 2012; Han *et al.* 2007).

The inflow rate greatly affected the contact between the adsorbate and adsorbent, which can be described by the fact that the residence time of the adsorbate was longer at a lower inflow rate and so, the adsorbent had longer time to bind As(V) oxyanions effectively (Podder, Majumder 2016; Lim, Aris 2014). On the other hand, the As(V) influent might have leaved the column before the equilibrium was reached, if the residence time of As(V) oxyanions in the PC-Fe/C column was not long enough to reach the adsorption equilibrium at a high inflow rate. Therefore, the adsorption was incomplete and a steep breakthrough curve was observed at the beginning of operation (Podder, Majumder 2016; Xu *et al.* 2013).

2.2.3. Effect of influent pH

The adsorption capacity, efficiency and mechanism from water onto the adsorbent surface are related to the influent pH, which affected the physical-chemical interaction between the aqueous adsorbate species and the adsorptive sites on the adsorbent surface (Targan *et al.* 2013; Aksu, Gönen 2004). The As(V) adsorption experiments were carried out at the pHs between 1.0 and 10.0 to examine the effect of the influent pHs on As(V) adsorption in the PC-Fe/C column using a plot of dimensionless concentration (C_t/C_0) versus time (t) (Figure 6). The equilibrium As(V) uptake (q_e) and the total As(V) removal efficiency (Y) at different influent pHs were also listed in Table 1. The adsorption removal of As(V) was more efficient at the low influent pHs than at the high influent pHs. The highest adsorption capacity and removal rate for As(V) appeared at the influent pH 3, i.e., 10.49 mg/g and 71.63%, respectively. They decreased significantly with the influent pH increase from 3 to 10. The times needed for the 50%

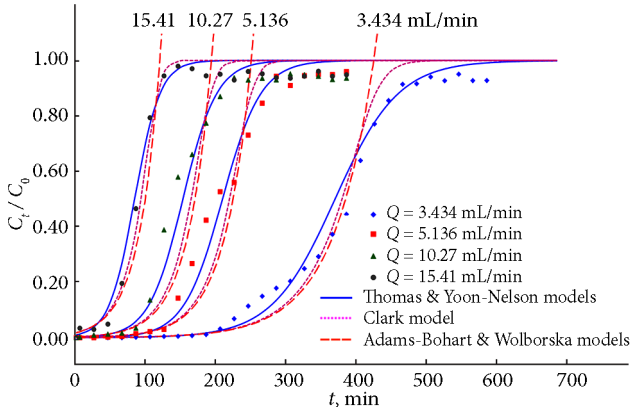

Figure 5. Effect of influent flow rate on breakthrough curve for As(V) adsorption removal by the PC-Fe/C adsorbent prepared with eucalyptus wood template (influent As(V) concentration: 20 mg/L; pH: 3; adsorbent mass: 2 g; adsorbent grain size: <100 mesh; operating temperature: 35 °C)

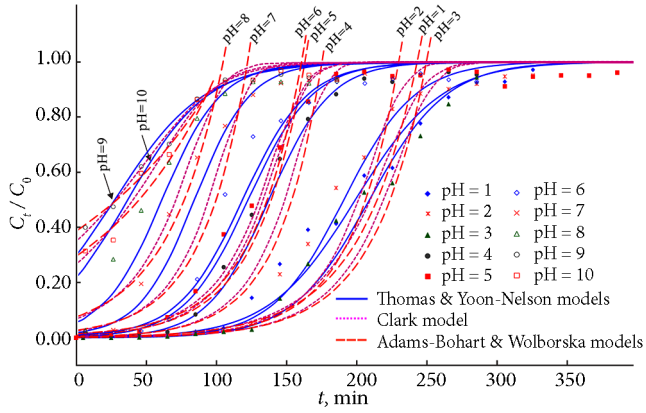

Figure 6. Effect of influent pH on breakthrough curve for As(V) adsorption removal by the PC-Fe/C adsorbent prepared with eucalyptus wood template (influent As(V) concentration: 20 mg/L; flow rate: 5.136 mL/min; adsorbent mass: 2 g; adsorbent grain size: <100 mesh; operating temperature: 35 °C)

adsorbate breakthrough (τ_{exp}) decreased significantly with the increasing influent pHs (Figure 6 and Table 2), which indicated that the breakthrough curves shifted clearly with the increasing influent pH.

2.2.4. Effect of adsorbent mass (bed depth)

The contact time of the influent along the column bed decreased with the decreasing adsorbent mass (bed depth), although the influent rate was kept same (Podder, Majumder 2016). To determine the effects of adsorbent mass (bed depth) on the breakthrough time, 20 mg/L As(V) solution of pH 3.0 was inlet through the PC-Fe/C column at an inflow rate of 5.136 mL/min by varying the adsorbent mass (bed depth). The breakthrough for As(V) happened earlier and the bed column exhausted faster with the decreasing adsorbent mass, i.e., the column breakthrough time was greatly influenced by the bed depth (Lim, Aris 2014). The increase of the As(V) adsorption capacity with the increasing adsorbent mass might be owing to the increased surface area of the adsorbent that could offer more binding sites for adsorption (Podder, Majumder 2016; Han *et al.* 2007). The larger adsorbent amount could delay the bed exhaustion time, which meant that the PC-Fe/C bed column could operate for a longer time without replacing the adsorbent (Podder, Majumder 2016; Xu *et al.* 2013).

The breakthrough curves for variation in the amount of the PC-Fe/C (adsorbent mass: 1, 2, 3, 4 g or bed depth: 0.85, 1.69, 2.54, 3.38 cm) loaded into the adsorption column are plotted in Figure 7. As the adsorbent mass or the bed depth was increased, As(V) had a longer time to be adsorbed onto PC-Fe/C with a higher removal efficiency. Thus, the larger adsorbent mass could cause a decrease in the effluent As(V) concentration within the same operating time. The slopes of the breakthrough curves increased with the decreasing adsorbent mass, which resulted in a broadened mass transfer zone (Han *et al.* 2007).

The equilibrium As(V) uptakes (q_e) and the total As(V) removal efficiencies (Y) versus the adsorbent mass are presented in Table 1. As the adsorbent mass (bed depth) decreased, the breakthrough for As(V) occurred earlier and the bed column exhausted faster. The increase in adsorbent mass could improve the column operation and reduce the effluent As(V) concentration at the end of the system (Table 1 and 2). The result showed that the throughput capacity of the As(V) solution increased with the increase in adsorbent mass or bed depth due to the accessibility of more adsorption sites (Nwabanne, Igbokw 2012). For a larger adsorbent mass, the effluent As(V) concentration decreased more rapidly than for a smaller adsorbent mass. Additionally, the beds were saturated in a longer time for a larger adsorbent mass. An increase in the adsorbent mass increased the service area of the adsorbent bed (Auta *et al.* 2013). The operation area increase enhanced more interaction between As(V) oxyanions and the active sites on PC-Fe/C, gave a prolonged breakthrough point attainment, henceforth increased the treatment volume of the As(V) influent and the adsorption capacity.

2.2.5. Effect of adsorbent grain size

Effects of adsorbent grain sizes were studied with various adsorbent grain sizes, while the other conditions were kept constant (Figure 8, Table 1 and 3). The adsorption of As(V) was greatly related to the adsorbent grain size. The equilibrium adsorption capacities [$q_{e,exp}$] were 4.51 mg/g, 6.11 mg/g, 6.60 mg/g, 7.57 mg/g and 10.49 mg/g for the adsorbent grain sizes of 20~40 mesh (0.841~0.4 mm), 40~60 mesh (0.4~0.25 mm), 60~80 mesh (0.25~0.177 mm), 80~100 mesh (0.177~0.149 mm) and <100 mesh (<0.149 mm), respectively. The total As(V) removal efficiencies increased from 53.20% to 71.63% with the decreasing adsorbent grain sizes. The influent volume treated was the largest for the smallest grain size (<100 mesh or <0.149 mm). As the adsorbent grain sizes decreased, flatter breakthrough curves and later breakthrough times were observed because the adsorbent

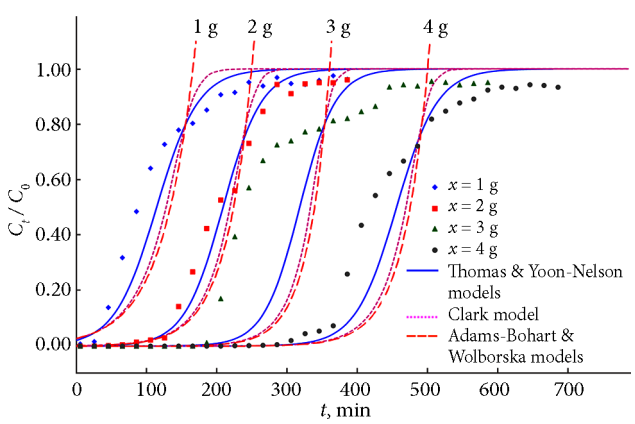

Figure 7. Effect of adsorbent mass on breakthrough curve for As(V) adsorption removal by the PC-Fe/C adsorbent prepared with eucalyptus wood template (influent As(V) concentration: 20 mg/L; flow rate: 5.136 mL/min; pH: 3; adsorbent grain size: <100 mesh; operating temperature: 35 °C)

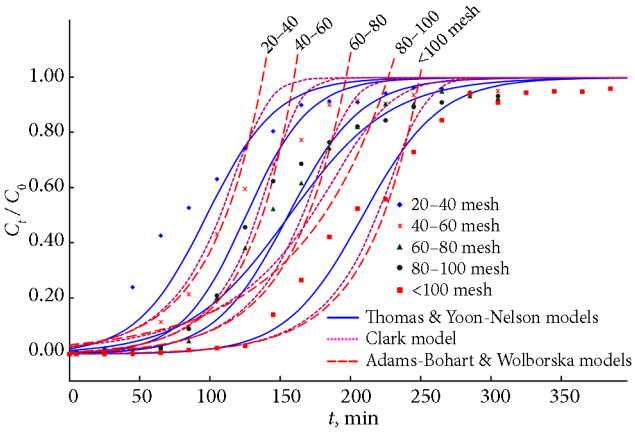

Figure 8. Effect of adsorbent grain size on breakthrough curve for As(V) adsorption removal by the PC-Fe/C adsorbent prepared with eucalyptus wood template (influent As(V) concentration: 20 mg/L; flow rate: 5.136 mL/min; pH: 3; adsorbent mass: 2 g; operating temperature: 35 °C)

surface area increased and the adsorption sites were more gradually occupied in the PC-Fe/C column. The times required for 50% As(V) breakthrough (τ_{exp}) were 80 min, 114 min, 142 min, 130 min and 200 min for the adsorbent grain sizes of 20~40 mesh, 40~60 mesh, 60~80 mesh, 80~100 mesh and <100 mesh, respectively (Table 2).

2.2.6. Effect of operating temperature

The breakthrough curves for the As(V) adsorption by PC-Fe/C at different operating temperatures and their adsorption capacities are illustrated in Figure 9 and Table 1 and 2. The equilibrium adsorption capacities ($q_{e,exp}$) were 9.16 mg/g, 10.49 mg/g and 11.01 mg/g, and the times required for 50% adsorbate breakthrough (τ_{exp}) were 180 min, 200 min and 208 min at the operating temperatures of 25, 35 and 45 °C, respectively. The As(V) adsorption was not significantly influenced by the operating temperature, i.e., the breakthrough curve shifted not obviously with the variation of the operating temperature. Thus, the PC-Fe/C adsorbent could be used for As(V) removal over a wide range of operating temperature.

2.3. Arsenate adsorption mechanisms

The arsenate adsorption is strongly dependent on the point of zero charge of adsorbents (pH_{PZC}), at which the net charge of the adsorbent surface is neutral. When the pH_{PZC} value is higher than the solution pH, the particle surface is positively charged; when the pH_{PZC} value is lower than the solution pH, the particle surface is negatively charged. The pH_{pzc} values of the PC-Fe/C adsorbent, Fe_3O_4, α-Fe_2O_3 and the eucalyptus wood biochar were 3.2, 5.7, 5.2, and 3.1, respectively. The pH_{PZC} of the PC-Fe/C adsorbent (3.2) was lower than that of magnetite and hematite. In the acidic aqueous solution, the iron oxides surface is positively charged.

The amount of the positively charged sites on the adsorbent particle surface together with arsenate speciation determined the pH reliance of arsenate adsorption by magnetite and hematite. The change of the concentration of each arsenic(V) species with pH indicated that As(V) exists mainly as negatively charged arsenate anions [$H_2AsO_4^-$, $HAsO_4^{2-}$ or AsO_4^{3-}], accounting for more than 99 per cent of the total As(V) in solution, which can be strongly adsorbed onto the positively charged surface sites of iron oxides when the solution pH is lower than their pH_{PZC} (Figure 10). Only in strong acidic solution, some part of As(V) can exist as neutral molecules, i.e., H_3AsO_4 species.

The solution pH can also affect the ionization of all functional groups existing on the adsorbent surface simultaneously. When pH <5.6 (pK_{a1}), main functional groups on the solid surface are Fe^{2+} or $FeOH^+$, i.e., magnetite can attract negatively charged species. When pH >5.6, the main functional hydroxyl groups on the solid surface are $Fe(OH)_3^-$ and $Fe(OH)_2^0$, the negatively charged adsorbent surface repelled negatively charged species (Zhu *et al.* 2013). The As(V) adsorption onto magnetite and hematite may involve many chemical reactions (Zhu *et al.* 2013), i.e., forming of the mono-dentate inner sphere complexes on iron oxides through replacing of the singly coordinated surface hydroxyl groups by the arsenate species $HAsO_4^{2-}$ (10); protonation of the arsenate species adsorbed (11, 12), and deprotonation and protonation of the singly coordinated surface hydroxyl (12, 13). In the present work, the protonation reactions (11, 12, 13) occurred when pH <6.8 and the H^+ consumption caused a pH increase. When pH >6.8, the deprotonation reaction (14) occurred and the solution pH decreased (Figure 10).

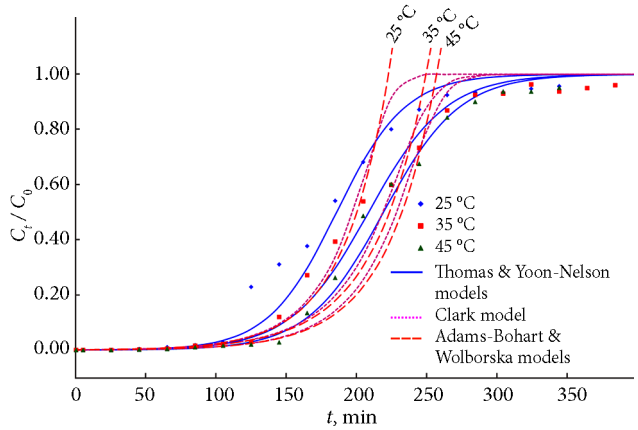

Figure 9. Effect of temperature on breakthrough curve for As(V) adsorption removal by the PC-Fe/C adsorbent prepared with eucalyptus wood template (influent As(V) concentration: 20 mg/L; flow rate: 5.136 mL/min; pH: 3; adsorbent mass: 2 g; adsorbent grain size: <100 mesh)

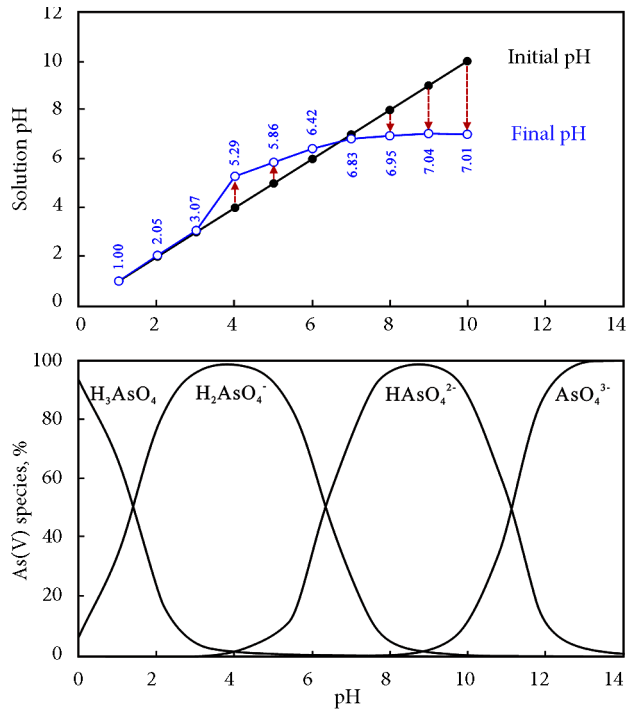

Figure 10. Variation of the As(V) species distribution with solution pHs (As(V) = 20 mg/L, 35 °C)

$$\equiv Fe–OH + HAsO_4^{2-} = \equiv Fe–AsO_4^{2-} + H_2O; \quad (10)$$

$$\equiv Fe–AsO_4^{2-} + H^+ = \equiv Fe–AsO_4H^-; \quad (11)$$

$$\equiv Fe–AsO_4H^- + H^+ = \equiv Fe–AsO_4H_2; \quad (12)$$

$$\equiv Fe–OH + H^+ = \equiv Fe–OH_2^+; \quad (13)$$

$$\equiv Fe–OH = \equiv Fe–O^- + H^+. \quad (14)$$

2.4. Adsorption modeling for breakthrough curve

2.4.1. The Thomas model and the Yoon–Nelson model

The Thomas rate constants (k_{Th}) and the equilibrium As(V) uptakes ($q_{e,\ calc}$) were calculated by fitting the column experimental data to the Thomas model (Table 1). Together with the experimental data points under different experimental conditions, the curves predicted by the Thomas equation are also illustrated in Figures 4~10, respectively. The coefficients (R^2) values for linear regression ranged from 0.8367 to 0.9907, which showed a significant correlation between C_t/C_0 and t (Table 1).

The Thomas rate constants (k_{Th}) decreased with the increasing influent As(V) concentration and increased with the increasing inflow rates. The concentration difference between As(V) in the solution and As(V) on the adsorbent surface was the driving force for adsorption. Hence, the higher influent As(V) concentration resulted in the higher driving force and a better column performance. Lower inflow rate and higher influent As(V) concentration could enhance the As(V) adsorption in the PC-Fe/C column. Longer residence times at lower inflow rates allowed for longer diffusion of the As(V) ions. The k_{Th} values increased from 0.00111 mL/min·mg to 0.00277 mL/min·mg with the increasing inflow rate from 3.434 mL/min to 15.41 mL/min. The influent pH, adsorbent mass (bed depth), adsorbent grain size and operating temperature had little effect on the Thomas rate constant (k_{Th}). The calculated equilibrium As(V) uptakes ($q_{e,calc}$) were nearly the same as the experimental values ($q_{e,exp}$) (Table 1). The predicted and the experimental data were plotted with great consistency (Figures 4~10). The Thomas model was suitable to describe the As(V) adsorption process, in which the external and internal diffusions were not the limiting step.

The Yoon–Nelson model, which is a simple theoretical model because less column data are required to construct the model, was also applied to examine the breakthrough characters of the As(V) adsorption onto PC-Fe/C. The Yoon–Nelson rate constants (k_{YN}) and the times required for 50% As(V) breakthrough (τ) were calculated and listed in Table 2. The results indicated that the k_{YN} values increased with the increasing influent concentrations and inflow rates. The 50% breakthrough times (τ) decreased with the increasing influent As(V) concentrations and the increasing inflow rates, and increased with the increasing adsorbent mass. The calculated τ values (τ_{calc}) were near to the experimental results (τ_{exp}). The deviation of τ_{calc} from τ_{exp} ($\Delta\tau/\tau_{exp}$) was determined to be 4.34% under the conditions of the influent As(V) concentration 20 mg/L, inflow rate 5.136 mL/min, pH 3, adsorbent mass 2 g, adsorbent grain size <100 mesh and operating temperature 35 °C (Table 2). In order to compare with the experimental data points, the predicted curves from the Yoon–Nelson model are also plotted in Figures 4~10.

The increase of the rate constants (k_{YN}) and the adsorption capacities (q_e) with the increasing influent As(V) concentrations is considered to be owing to the increasing competition of As(V) ions for the adsorption sites on the PC-Fe/C surface, which lastly resulted in the increase of the As(V) uptake rates (Nwabanne, Igbokw 2012). The high correlation coefficients (R^2 = 0.8367 to 0.9907) indicated that the experimental data could be well fitted with the Yoon–Nelson equation. Table 1 and Table 2 show that the correlation coefficients (R^2) for the Yoon-Nelson model were the same as that for the Thomas model when the linear regression was used. Therefore, the Thomas and Yoon-Nelson models can very well describe the As(V) adsorption onto the PC-Fe/C surface.

The Yoon-Nelson rate constants (k_{YN}) increased with the increasing adsorbent mass from 1 g to 3 g. Due to the high linear regression coefficients for the plotted curves of the influent flow rate (Q) or adsorbent mass (x) versus the Yoon-Nelson model parameters [τ_{Theo}, t_1 and t_2], the breakthrough times and exhaustion times for the adsorption breakthrough curves were calculated (Appendix C, D). The dynamic adsorption capacity were also calculated to be 11.73 mg/g, 10.72 mg/g, 10.88 mg/g and 11.70 mg/g for the adsorbent masses of 1 g, 2 g, 3 g and 4 g, respectively, which were close to the experimental data (Table 1).

2.4.2. The Clark model

It was confirmed that the Freundlich equation could be used to express the As(V) adsorption on the PC-Fe/C adsorbent in a previous batch research (Wei *et al.* 2013). So, the Freundlich constants $1/n$ (0.1916, 25 °C; 0.2304, 35 °C; 0.2252, 45 °C) were used to estimate the parameters of the Clark model. The A and r values of the Clark model were calculated according to Eq. (7) by the means of the linear regression analysis and are showed in Appendix A. As the influent As(V) concentration and the inflow rate increased, the constants of the Clark model (A) decreased and the adsorption rates (r) increased. The breakthrough curves predicted by the Clark model according to Eq. (7) were also plotted in Figures 4~10. The results indicated that the predicted curves had a good correlation with the experimental data points in respects of the effects of the influent As(V) concentration (R^2 = 0.7364~0.9781), the inflow rate (R^2 = 0.9314~0.9515), the adsorbent mass (R^2 = 0.7633~0.9314) and the adsorbent grain size (R^2 = 0.7761~0.9314).

2.4.3. The Adams–Bohart model and the Wolborska model

The Adams–Bohart and Wolborska adsorption models could be used to describe the initial part of the breakthrough curves (Figures 4~10, Appendix B). As the influent As(V) concentration increased from 10 mg/L to 50 mg/L,

the kinetic constant k_{AB} of the Adams–Bohart model decreased from 0.001320 L/mg·min to 0.000714 L/mg·min and the kinetic coefficient of the external mass transfer (β_a) of the Wolborska model decreased from 0.0149 to 0.0100 1/min. As the influent flow rate increased from 3.434 mL/min to 15.41 mL/min, the kinetic constant k_{AB} of the Adams–Bohart model increased from 0.000865 to 0.001675 L/mg·min and the kinetic coefficient of the external mass transfer (β_a) of the Wolborska model increased from 0.0116 to 0.0282 1/min. This indicated that the external mass transfer was the dominant kinetics in the initial part of As(V) adsorption in the column system. The experimental data under different experimental conditions were compared with the predicted curves using the Adams–Bohart model and the Wolborska model in Figures 4~10. There was a good correlation between the experimental data and the predicted curves in the initial part of the column adsorption. The Adams–Bohart and Wolborska models were valid only for the relative As(V) concentration up to 60% breakthrough, and there was a great divergence between the experimental data and the predicted curves above this value.

2.4.4. Comparison of the five models

When a linear regression was used during fitting, the correlation coefficients (R^2) for the Thomas model were the same as those for the Yoon–Nelson model and the correlation coefficients (R^2) for the Adams–Bohart model were the same as those for the Wolborska model. The Thomas and Yoon–Nelson models could well describe the behavior of the adsorption process, but the Adams–Bohart, Wolborska and Clark models did not offer the best results. Comparing the correlation coefficients (R^2) for the five models, the correlation coefficients (R^2) for the Thomas and Yoon–Nelson models were 0.9807 under the conditions of the influent As(V) concentration 20 mg/L, inflow rate 5.136 mL/min, pH 3, adsorbent mass 2 g, adsorbent grain size <100 mesh and operating temperature 35 °C, which were higher than 0.9314 for the Clark model and 0.9058 for the Adams–Bohart and Wolborska models. Therefore, the Thomas and Yoon–Nelson models were better in describing the As(V) adsorption process in the PC-Fe/C column. Regarding the Adams–Bohart and Wolborska models, they could predict only the initial part of the breakthrough curves. In the present work, the predicted range was up to C_t/C_0 = 0.6, and the correlation coefficients (R^2) were smaller than those for the Thomas and Yoon–Nelson models under the same experimental conditions.

2.5. Comparison of adsorption capacity

Table 3 presents a comparison of the PC-Fe/C adsorbent with some iron oxides and iron-oxide-coated adsorbents for the arsenate adsorption removal from water in

Table 3. Comparison of adsorption capacity of the PC-Fe/C adsorbent with some iron oxides for As(V) removal

Adsorbent	pH	As(V) Concentr. (mg/L)	Surface area (m^2/g)	Grain size (mm)	Capacity (mg/g)	Ref.
PC-Fe/C	3	20	198.1	<0.149	**9.31–14.99**	This study
α-Fe_2O_3	3	5–50	–	<0.25	0.33–1.63	This study
Magnetite	6.5	0.075–75	0.89	0.1	0.12	Giménez *et al.* 2007
Magnetite	6	0.075–15	1.6	–	0.85	Mamindy-Pajany *et al.* 2011
Magnetite	4	0.5	–	28 nm	1.58	Parsons *et al.* 2009
Magnetite	6	0.3–100	–	17 nm	4.78	Luther *et al.* 2012
Magnetite	4.8–6.1	0–33.71	3.7	300 nm	0.75–1.08	Yean *et al.* 2005
Magnetite	4.8–8	0–33.71	60	20 nm	5.95–11.41	Yean *et al.* 2005
Magnetite 98%	5	5	6.58	–	0.05	Aredes *et al.* 2012
Hematite	7.3	0.075–75	0.38	0.25	0.10	Giménez *et al.* 2007
Hematite	6	0.075–15	1.66	0.05	0.41	Mamindy-Pajany *et al.* 2011
Hematite	6	0.3–100	–	12 nm	4.90	Luther *et al.* 2012
Hematite 96–98%	5	5	3.77	–	0.21	Aredes *et al.* 2012
Hematite 80.8%	4.2	10	14.4	0.200	0.20	Singh *et al.* 1996
Goethite	7.5	0.075–75	2.01	0.25	0.20	Giménez *et al.* 2007
Goethite	6	0.075–15	11.61	0.01	1.218	Mamindy-Pajany *et al.* 2011
Goethite 99%	5	5	12.1	–	0.05	Aredes *et al.* 2012
Iron oxide pillared clays	6	0.2~2	275	–	0.026	Mishra, Mahato 2016
Iron-impregnated biochar	5.8	0.1–55	16	–	2.16	Hu *et al.* 2015
Fe-hydrotalcite supported magnetite nanoparticle	9	0.1~2	–	50 nm	1.28	Türk, Alp 2014
ACs modified with Fe hydro(oxide) nanoparticles	6–8	0.025–1.5	1045	3–36 nm	0.37–1.25	Vitela-Rodriguez, Rangel-Mendez 2013

literatures (Giménez *et al.* 2007; Mamindy-Pajany *et al.* 2011; Parsons *et al.* 2009; Luther *et al.* 2012; Yean *et al.* 2005; Aredes *et al.* 2012; Singh *et al.* 1996; Mishra, Mahato 2016; Hu *et al.* 2015; Türk, Alp 2014; Vitela-Rodriguez, Rangel-Mendez 2013).

As shown in the table, the PC-Fe/C adsorbent has a significant potential for the adsorption removal of As(V) from aqueous solution. The adsorption capacity of the PC-Fe/C adsorbent for As(V) (9.31~14.99 mg/g) was higher than those of natural hematite (0.10 mg/g), natural magnetite (0.12 mg/g) and natural goethite (0.20 mg/g) (Giménez *et al.* 2007). Additionally, the As(V) adsorption capacities were 0.85, 0.41 and 1.22 mg/g for commercial magnetite, hematite and goethite, respectively (Mamindy-Pajany *et al.* 2011). The As(V) adsorption capacities (9.31~14.99 mg/g) were 5.91~9.52 times 1.575 mg/g, which was reported to be the As(V) adsorption capacity for the synthetic magnetite nano-adsorbent (Parsons *et al.* 2009). Additionally, the PC-Fe/C adsorbent also showed a higher As(V) adsorption capacity than iron-oxide-coated adsorbents, such as activated carbons modified with iron hydro (oxide) nanoparticles (Vitela-Rodriguez 2013), Fe-hydrotalcite supported magnetite nanoparticle (Türk, Alp 2014), iron-impregnated biochar (Hu *et al.* 2015) and iron oxide pillared clays (Mishra, Mahato 2016).

A decreasing of the specific surface areas from 256 m^2/g for biochar to 16.0 m^2/g for Fe-impregnated biochar suggested that Fe-impregnation could clog pore-openings or fill pores on biochar surfaces (Hu *et al.* 2015). The soaking–drying process of the present work has overcome this disadvantage. The As(V) adsorption capacity of the commercially obtainable 20-nm magnetite (5.95~11.41 mg/g) was nearly 8~10 times that of the commercially obtainable 300-nm magnetite (0.75~1.08 mg/g) (Yean *et al.* 2005). Normally, the finer the grain size the greater the adsorption capacity. Nevertheless, nano-materials tend to aggregate in water, which might limit their adsorption effectiveness and their large-scale application (Xu *et al.* 2013). Although the removal rate was the highest with the smallest particle size, it is not suitable for the fixed-bed column application, due to potential clogging and serious hydraulic obstruction when waste streams flow through columns (Guo *et al.* 2014). Hence, the hierarchical porous microstructure of the PC-Fe/C adsorbent prepared with eucalyptus wood template has a beneficial effect on the overall adsorption when the adsorbent is used without additional grinding to nanoparticles.

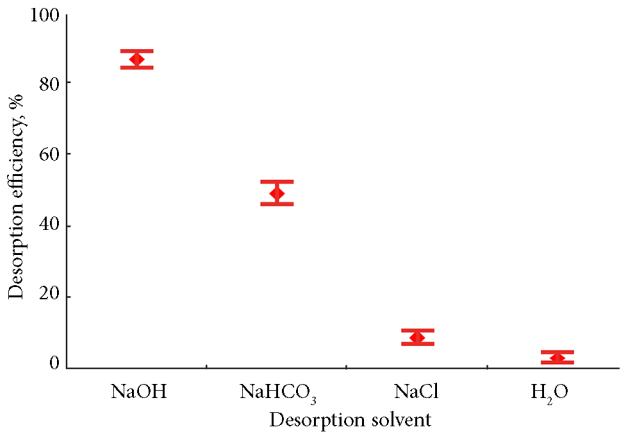

Figure 11. Effect of desorption solvent types on the As(V) desorption efficiencies

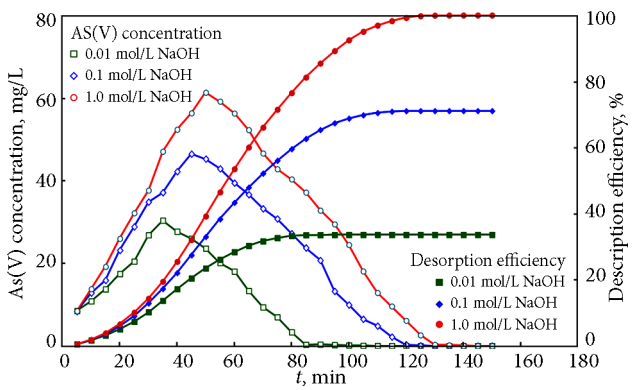

Figure 12. Effect of eluent concentration on the As(V) desorption efficiencies (flow rate: 5.136 mL/min; adsorbent mass: 2 g; adsorbent grain size: <100 mesh; operating temperature: 35 °C)

2.6. Column desorption and regeneration

2.6.1. Effect of desorption eluent

Desorption of the As(V) (adsorbate) from the PC-Fe/C adsorbent was carried out using four different eluents, i.e., 0.1 mol/L NaOH, 0.1 mol/L $NaHCO_3$, 0.1 mol/L NaCl and 0.1 mol/L H_2O. The desorption efficiencies were 86.84%, 49.35%, 8.81% and 2.73% for 0.1 mol/L NaOH, 0.1 mol/L $NaHCO_3$, 0.1 mol/L NaCl and 0.1 mol/L H_2O, respectively (Figure 11). The 0.1 mol/L NaOH solution was more effective than others (Figure 11), which was owing to the lower As(V) adsorption at a higher pH (pH >10) (Wei *et al.* 2013). As indicated previously (Figure 7), As(V) exists as negatively charged arsenate anions [AsO_4^{3-} and $HAsO_4^{2-}$] in more alkaline solution at pH >10 (Yu *et al.* 2013; Sarı *et al.* 2010), while a negative surface of the PC-Fe/C adsorbent formed at the same pH, which resulted in a desorption of As(V) from the PC-Fe/C adsorbent. Therefore, NaOH solution was used as desorption solution in the following column regeneration test.

2.6.2. Effect of desorption eluent concentration

The column desorption of As(V) from the PC-Fe/C adsorbent was studied at different inflow concentrations of NaOH, i.e., 0.01, 0.1 and 1.0 mol/L under the same conditions of the influent flow rate of 5.136 mL/min, the adsorbent mass of 2 g, the adsorbent grain size of <100 mesh and the operating temperature of 35 °C. The results obtained for three different NaOH concentrations are showed in Figure 12. The maximum As(V) concentrations in the effluent were 61.28 mg/L for 1.0M NaOH, 46.43 mg/L for 0.1M NaOH and 30.33 mg/L for 0.01M NaOH after operating for 50, 45 and 35 min, respectively.

The total regeneration efficiencies after the 140min desorption were near 100% for 1.0M NaOH, 71.75% for 0.1M NaOH and 33.94% for 0.01M NaOH, i.e., the regeneration efficiencies increased with the increasing eluent concentrations. During the desorption with 1M NaOH, the surfaces of the adsorbents became more negative, and the percentage of AsO_4^{3-} and $HAsO_4^{2-}$ species also increased in high alkaline solutions. However, 0.1M NaOH may be more appropriate as eluent in the actual desorption performance because of severe problems caused by disposal of a higher basic waste.

2.6.3. Effect of inflow rate

The column desorption of As(V) from the PC-Fe/C adsorbent was made at three influent flow rates, i.e., 3.43 mL/min, 5.14 mL/min and 10.27 mL/min, under the conditions of the eluent concentration of 0.1 mol/L NaOH, the adsorbent mass of 2 g, the adsorbent grain size of <100 mesh and the operating temperature of 35 °C. The results obtained for the three different influent flow rates are shown in Figure 13. The highest concentrations of As(V) in the effluent solutions were 50.42 mg/L at the inflow rate of 3.43 mL/min after operating for 75 min, 46.43 mg/L at 5.14 mL/min after 45 min and 30.82 mg/L at 10.27 mL/min after 30 min. The total regeneration efficiencies were 66.79% at the eluent inflow rate of 3.43 mL/min after desorption for 175 min, 71.75% at 5.14 mL/min after 140 min and 58.82% at 10.27 mL/min after 95 min, respectively.

2.6.4. Effect of operating temperature

The column desorption of As(V) from the PC-Fe/C adsorbent was carried out at the temperatures of 25 °C, 35 °C and 45 °C, under the conditions of the eluent concentration of 0.1 mol/L NaOH, the inflow rate of 5.136 mL/min, the adsorbent mass of 2 g and the adsorbent grain size of <100 mesh. The results obtained for three different operating temperatures are showed in Figure 14. The highest As(V) concentrations in the effluents were 40.07 mg/L after operating at 25 °C for 50 min, 46.43 mg/L after operating at 35 °C for 45 min and 50.21 mg/L after operating at 45 °C for 50 min. The total regeneration efficiencies were 51.75% at 25 °C after the desorption operating for 130 min, 71.75% at 35 °C after 140min and 80.98% at 45 °C after 135 min, respectively, i.e., the regeneration efficiencies increased slightly with the increasing operating temperature.

Conclusions

The PC-Fe/C adsorbent can be applied to remove As(V) from water efficiently. The increase in the adsorbent mass (bed depth) and the decrease in the adsorbent grain size could greatly affect the column performance by decelerating the exhaustion time and improve the column quality. The total removal efficiency of As(V) increased with the increasing adsorbent mass. The increase in the influent flow rate, the influent As(V) concentration and the influent pH tended to accelerate the column exhaustion. The operating temperature had negligible influence on the column As(V) removal.

The Thomas and Yoon–Nelson models presented a very good correlation for the As(V) experimental data ($R^2 > 0.9$). The models can accurately predict the operation status of the adsorbent columns under the conditions of various As(V) influent concentrations, inflow rates, adsorbent masses and operating temperatures. The experimental and theoretical data were obviously correlated including the column parameters q_e, τ, t_1 and t_2. The times required for 50% breakthrough (τ) decreased with the increasing influent As(V) concentration, inflow rate and adsorbent mass (bed depth). The Adams–Bohart and Wolborska models were observed only suitable to express the initial part of the breakthrough curves. Under the condition of the influent As(V) concentration of 20 mg/L, the influent flow rate of 5.136 mL/min, the influent pH of 3, the adsorbent mass of 2 g, the adsorbent grain size of <100 mesh and the operating temperature of 35 °C, the equilibrium adsorption capacity reached 10.49 mg/g, which was near the predicted value of 10.72 mg/g according to the Thomas model.

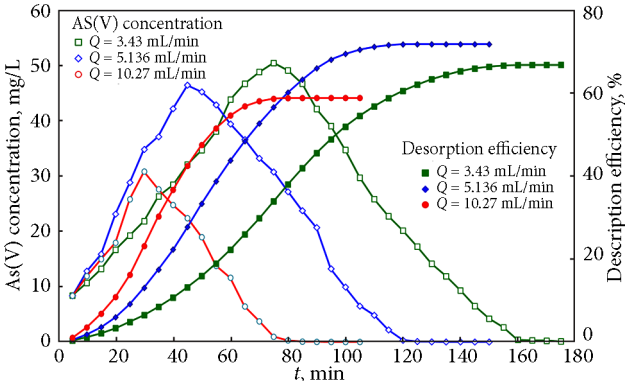

Figure 13. Effect of flow rate on the As(V) desorption efficiencies (eluent concentration: 0.1 mol/L NaOH; adsorbent mass: 2 g; adsorbent grain size: <100 mesh; operating temperature: 35 °C)

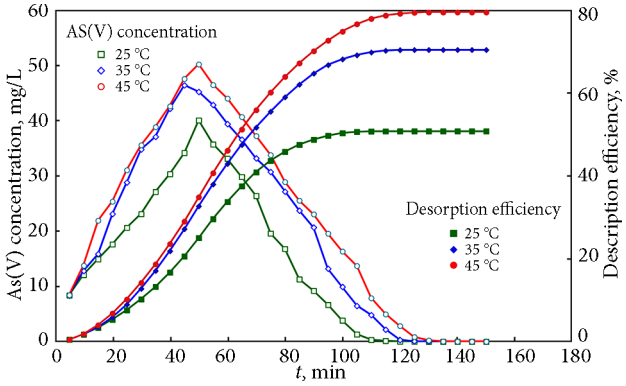

Figure 14. Effect of operating temperature on the As(V) desorption efficiencies (eluent concentration: 0.1 mol/L NaOH; flow rate: 5.136 mL/min; adsorbent mass: 2 g; adsorbent grain size: <100 mesh)

The column desorption of the adsorbed As(V) from PC-Fe/C were greatly depended on the eluent concentration, inflow rate and operating temperature. After the desorption operating for 140 min by using 1M NaOH at the inflow rate of 5.136 mL/min, >99% of the adsorbed As(V) could be effectively eluted.

Acknowledgements

The manuscript has greatly benefited from insightful comments by the editor and anonymous reviewers. The authors thank the Guangxi Key Laboratory of Environmental Pollution Control Theory and Technology for the research assistance. This research was financially assisted by the National Natural Science Foundation of China (NSFC 21707024, 41763012, 51638006), the Guangxi Science and Technology Development Project (GuiKeGong14124004-3-3) and the Provincial Natural Science Foundation of Guangxi (2014GXNSFBA118054).

References

Acosta, J. A.; Arocena, J. M.; Faz, A. 2015. Speciation of arsenic in bulk and rhizosphere soils from artisanal cooperative mines in Bolivia, *Chemosphere* 138: 1014–1020. https://doi.org/10.1016/j.chemosphere.2014.12.050

Aksu, Z.; Gönen, F. 2004. Biosorption of phenol by immobilized activated sludge in a continuous packed bed: prediction of breakthrough curves, *Process Biochemistry* 39(5): 599–613. https://doi.org/10.1016/S0032-9592(03)00132-8

Aredes, S.; Klein, B.; Pawlik, M. 2012. The removal of arsenic from water using natural iron oxide minerals, *Journal of Cleaner Production* 29–30: 208–213. https://doi.org/10.1016/j.jclepro.2012.01.029

Auta, M.; Amat Darbis, N. D.; Mohd Din, A. T.; Hameed, B. H. 2013. Fixed-bed column adsorption of carbon dioxide by sodium hydroxide modified activated alumina, *Chemical Engineering Journal* 233: 80–87. https://doi.org/10.1016/j.cej.2013.08.012

Banerji, T.; Chaudhari, S. 2016. Arsenic removal from drinking water by electrocoagulation using iron electrodes- an understanding of the process parameters, *Journal of Environmental Chemical Engineering* 4(4): 3990–4000. https://doi.org/10.1016/j.jece.2016.09.007

Chen, N.; Zhang, Z.; Feng, C.; Li, M.; Chen, R.; Sugiura, N. 2011. Investigations on the batch and fixed-bed column performance of fluoride adsorption by Kanuma mud, *Desalination* 268(1–3): 76–82. https://doi.org/10.1016/j.desal.2010.09.053

Ghosh, A.; Chakrabarti, S.; Ghosh, U. C. 2014. Fixed-bed column performance of Mn-incorporated iron(III) oxide nanoparticle agglomerates on As(III) removal from the spiked groundwater in lab bench scale, *Chemical Engineering Journal* 248: 18–26. https://doi.org/10.1016/j.cej.2014.03.010

Giménez, J.; Martínez, M.; de Pablo, J.; Rovira, M.; Duro, L. 2007. Arsenic adsorption onto natural hematite, magnetite, and goethite, *Journal of Hazardous Materials* 141(3): 575–580. https://doi.org/10.1016/j.jhazmat.2006.07.020

Goel, J.; Kadirvelu, K.; Rajagopal, C.; Garg, V. K. 2005. Removal of lead(II) by adsorption using treated granular activated carbon: batch and column studies, *Journal of Hazardous Materials* 125(1–3): 211–220. https://doi.org/10.1016/j.jhazmat.2005.05.032

Guo, X.; Wu, Z.; He, M.; Meng, X.; Jin, X.; Qiu, N.; Zhang, J. 2014. Adsorption of antimony onto iron oxyhydroxides: Adsorption behavior and surface structure, *Journal of Hazardous Materials* 276: 339–345. https://doi.org/10.1016/j.jhazmat.2014.05.025

Habuda-Stanić, M.; Kalajdžić, B.; Kuleš, M.; Velić, N. 2008. Arsenite and arsenateadsorption by hydrousferric oxide/polymeric material, *Desalination* 229(1–3): 1–9. https://doi.org/10.1016/j.desal.2007.06.034

Han, R.; Wang, Y.; Zou, W.; Wang, Y.; Shi, J. 2007. Comparison of linear and nonlinear analysis in estimating the Thomas model parameters for methylene blue adsorption onto natural zeolite in fixed-bed column, *Journal of Hazardous Materials* 145(1–2): 331–335. https://doi.org/10.1016/j.jhazmat.2006.12.027

Hu, X.; Ding, Z.; Zimmerman, A. R.; Wang, S.; Gao, B. 2015. Batch and column sorption of arsenic onto iron-impregnated biochar synthesized through hydrolysis, *Water Research* 68: 206–216. https://doi.org/10.1016/j.watres.2014.10.009

Lata, S.; Samadder, S. R. 2016. Removal of arsenic from water using nano adsorbents and challenges: A review, *Journal of Environmental Management* 166: 387–406. https://doi.org/10.1016/j.jenvman.2015.10.039

Lim, A. P.; Aris, A. Z. 2014. Continuous fixed-bed column study and adsorption modeling: Removal of cadmium (II) and lead (II) ions in aqueous solution by dead calcareous skeletons, *Biochemical Engineering Journal* 87(12): 50–61. https://doi.org/10.1016/j.bej.2014.03.019

Luther, S.; Borgfeld, N.; Kim, J.; Parsons, J. G. 2012. Removal of arsenic from aqueous solution: a study of the effects of pH and interfering ions using iron oxide nanomaterials, *Microchemical Journal* 101: 30–36. https://doi.org/10.1016/j.microc.2011.10.001

Mamindy-Pajany, Y.; Hurel, C.; Marmier, N.; Roméo, M. 2011. Arsenic(V) adsorption from aqueous solution onto goethite, hematite, magnetite and zero-valent iron: Effects of pH, concentration and reversibility, *Desalination* 281(20): 93–99. https://doi.org/10.1016/j.desal.2011.07.046

Mishra, T.; Mahato, D. K. 2016. A comparative study on enhanced arsenic(V) and arsenic(III) removal by iron oxide and manganese oxide pillared clays from ground water, *Journal of Environmental Chemical Engineering* 4(1): 1224–1230. https://doi.org/10.1016/j.jece.2016.01.022

Mohan, D.; Pittman, C. U. 2007. Arsenic removal from water/wastewater using adsorbents – A critical review, *Journal of Hazardous Materials* 142(1–2): 1–53. https://doi.org/10.1016/j.jhazmat.2007.01.006

Nwabanne, J. T.; Igbokwe, P. K. 2012. Adsorption performance of packed bed column for the removal of lead (II) using oil palm fibre, *International Journal of Applied Science and Technology* 2(5): 106–115.

Parsons, G. J.; Lopez, L. M.; Peralta-Videa, R. J.; Gardea-Torresdey, L. J. 2009. Determination of arsenic (III) and arsenic(V) binding to microwave assisted hydrothermal synthetically prepared Fe_3O_4, Mn_3O_4, and $MnFe_2O_4$ nanoadsorbents, *Microchemical Journal* 91(1): 100–106. https://doi.org/10.1016/j.microc.2008.08.012

Podder, M. S.; Majumder, C. B. 2016. Fixed-bed column study for As(III) and As(V) removal and recovery by bacterial cells immobilized on sawdust/$MnFe_2O_4$ composite, *Biochemical Engineering Journal* 105(2016) 114–135. https://doi.org/10.1016/j.bej.2015.09.008

Presas, J. M.; Pastor, Y.; Llorca, J.; Arellano-López, A. R.; Martínez-Fernández, J.; Sepúlveda, R. 2006. Microstructure and

fracture properties of biomorphic SiC, *International Journal of Refractory Metals and Hard Materials* 24(1–2): 49–54. https://doi.org/10.1016/j.ijrmhm.2005.07.003

Sabbatini, P.; Rossi, F.; Thern, G.; Marajofsky, A.; de Cortalezzi, M. M. F. 2009. Iron oxide adsorbers for arsenic removal: a low cost treatment for rural areas and mobile applications, *Desalination* 248(1–3): 184–192. https://doi.org/10.1016/j.desal.2008.05.104

Sarı, A.; Çıtak, D.; Tuzen, M. 2010. Equilibrium, thermodynamic and kinetic studies on adsorption of Sb(III) from aqueous solution using low-cost natural diatomite, *Chemical Engineering Journal* 162(2): 521–527. https://doi.org/10.1016/j.cej.2010.05.054

Sieber, H. 2005. Biomimetic synthesis of ceramics and ceramic composites, *Materials Science and Engineering A* 412(1): 43–47. https://doi.org/10.1016/j.msea.2005.08.062

Singh, D. B.; Prasad, G.; Rupainwar, D. C. 1996. Adsorption technique for the treatment of As(V)-rich effluents, *Colloids and Surfaces A: Physicochemical and Engineering Aspects* 111(1–2): 49–56. https://doi.org/10.1016/0927-7757(95)03468-4

Sinha, S.; Amy, G.; Yoon, Y.; Her, N. 2011. Arsenic removal from water using various adsorbents: magnetic ion exchange resins, hydrous ion oxide particles, granular ferric hydroxide, activated alumina, sulfur modified iron, and iron oxide-coated microsand, *Environmental Engineering Research* 16(3): 165–173. https://doi.org/10.4491/eer.2011.16.3.165

Smedley, P. L.; Kinniburg, D. G. 2002. A review of the source, behaviour and distribution of arsenic in natural waters, *Applied Geochemistry* 17(5): 517–568. https://doi.org/10.1016/S0883-2927(02)00018-5

Smith, A. E.; Lincoln, R. A.; Paulu, C.; Simones, T. L.; Caldwell, K. L.; Jones, R. L.; Backer, L. C. 2015. Assessing arsenic exposure in households using bottled water or point-of-use treatment systems to mitigate well water contamination, *Science of The Total Environment* 544: 701–710. https://doi.org/10.1016/j.scitotenv.2015.11.136

Targan, Ş.; Tirtom, V. N.; Akkuş, B. 2013. Removal of antimony(III) from aqueous solution by using grey and red Erzurum clay and application to the Gediz river sample, *ISRN Analytical Chemistry*, Article ID 962781. https://doi.org/10.1155/2013/962781

Türk, T.; Alp, İ. 2014. Arsenic removal from aqueous solutions with Fe-hydrotalcite supported magnetite nanoparticle, *Journal of Industrial and Engineering Chemistry* 20(2): 732–738. https://doi.org/10.1016/j.jiec.2013.06.002

Vitela-Rodriguez, A. V.; Rangel-Mendez, J. R. 2013. Arsenic removal by modified activated carbons with iron hydro (oxide) nanoparticles, *Journal of Environmental Management* 114: 225–231. https://doi.org/10.1016/j.jenvman.2012.10.004

Wei, W.; Zhu, Z.; Zhu, Y.; Qin, H.; Liang, M. 2013. Adsorption of Sb(III) from aqueous solution by the porous biomorph-genetic composite of Fe_2O_3-Fe_3O_4/C prepared with eucalyptus wood template, *Technology of Water Treatment* 39(5): 69–72 (in Chinese).

WHO. 2016. Arsenic [online], [cited 30 September 2016]. World Health Organization. Available from Internet: http://www.who.int/mediacentre/factsheets/fs372/en

Xu, X.; Gao, B.; Tan, X.; Zhang, X.; Yue, Q.; Wang, Y.; Li, Q. 2013. Nitrate adsorption by stratified wheat straw resin in lab-scale columns, *Chemical Engineering Journal* 226: 1–6. https://doi.org/10.1016/j.cej.2013.04.033

Yean, S.; Cong, L.; Yavuz, C. T.; Mayo, J. T.; Yu, W. W.; Kan, A. T.; Colvin, V. L.; Tomson, M. B. 2005. Effect of magnetite particle size on adsorption and desorption of arsenite and arsenate, *Journal of Materials Research* 20(12): 3255–3264. https://doi.org/10.1557/jmr.2005.0403

Yu, T.; Zeng, C.; Ye, M.; Shao, Y. 2013. The adsorption of Sb(III) in aqueous solution by Fe_2O_3-modified carbon nanotubes, *Water Science and Technology* 68(3): 658–664. https://doi.org/10.2166/wst.2013.290

Zhu, Y.; Zhu, Z.; Chen, Y.; Yang, F.; Qin, H.; Xie, L. 2013. Kinetics and thermodynamics of sorption for As(V) on the porous biomorph-genetic composite of α-Fe_2O_3/Fe_3O_4/C with eucalyptus wood hierarchical microstructure, *Water, Air & Soil Pollution* 224: Article Number 1589. https://doi.org/10.1007/s11270-013-1589-y

Zhu, Z. Q.; Zhu, Y. N.; Qin, H.; Li, Y. H.; Liang, Y. P.; Deng, H.; Liu, H. L. 2015. Preparation and properties of porous composite of hematite/magnetite/carbon with eucalyptus wood biotemplate, *Materials and Manufacturing Processes* 30(3): 285–291. https://doi.org/10.1080/10426914.2014.941478

APPENDIX A

Parameters of the Clark model using linear regression analysis for As(V) adsorption to PC-Fe/C under different conditions.

Influent concentr. C_0, mg/L	Flow rate Q, mL/min	Sorbent mass x, g	Sorbent grain size, mesh	Operating temp. T, °C	Influent pH	r, mg/L·min	A, min	R^2
10	5.136	2	<100	35	3	0.0460	2.00E+09	0.9781
20	5.136	2	<100	35	3	0.0938	7.60E+09	0.9314
30	5.136	2	<100	35	3	0.0967	7.84E+07	0.8948
50	5.136	2	<100	35	3	0.1278	1.70E+06	0.7364
20	3.434	2	<100	35	3	0.0598	6.41E+10	0.9515
20	5.136	2	<100	35	3	0.0938	7.60E+09	0.9314
20	10.27	2	<100	35	3	0.1047	2.61E+08	0.9344
20	15.41	2	<100	35	3	0.1238	8.92E+05	0.9487
20	5.136	1	<100	35	3	0.0778	1.89E+05	0.7633
20	5.136	2	<100	35	3	0.0938	7.60E+09	0.9314
20	5.136	3	<100	35	3	0.1121	1.57E+17	0.8128
20	5.136	4	<100	35	3	0.0969	4.99E+20	0.8291
20	5.136	2	20-40	35	3	0.0952	2.48E+05	0.7852
20	5.136	2	40-60	35	3	0.1083	1.80E+07	0.8586
20	5.136	2	60-80	35	3	0.0917	3.62E+07	0.8885
20	5.136	2	80-100	35	3	0.0571	1.69E+05	0.7761
20	5.136	2	<100	35	3	0.0938	7.60E+09	0.9314
20	5.136	2	<100	25	3	0.1333	4.94E+12	0.8643
20	5.136	2	<100	35	3	0.0938	7.60E+09	0.9314
20	5.136	2	<100	45	3	0.1004	9.44E+10	0.9604
20	5.136	2	<100	35	1	0.0853	5.19E+08	0.9261
20	5.136	2	<100	35	2	0.1027	8.58E+09	0.9436
20	5.136	2	<100	35	3	0.0938	7.60E+09	0.9314
20	5.136	2	<100	35	4	0.1147	2.28E+08	0.9460
20	5.136	2	<100	35	5	0.1043	1.00E+07	0.9684
20	5.136	2	<100	35	6	0.1027	5.53E+06	0.9295
20	5.136	2	<100	35	7	0.1139	3.85E+05	0.8642
20	5.136	2	<100	35	8	0.0971	8.15E+03	0.7560
20	5.136	2	<100	35	9	0.0451	3.08E+01	0.9886
20	5.136	2	<100	35	10	0.0543	7.73E+01	0.9758

APPENDIX B

Parameters of the Adams-Bohart and Wolborska model using linear regression analysis for As(V) adsorption to PC-Fe/C under different conditions.

Influent concentr. C_0, mg/L	Flow rate Q, mL/min	Sorbent mass x, g	Sorbent grain size, mesh	Operating temp. T, °C	Influent pH	Z, cm	U_0, cm/min	k_{AB}, L/mg·min	N_0, mg/L	β_a (= k_{AB}·N_0), 1/min	R^2
10	5.136	2	<100	35	3	1.69	3.99	0.001320	11.26	0.0149	0.9713
20	5.136	2	<100	35	3	1.69	3.99	0.001335	11.77	0.0157	0.9058
30	5.136	2	<100	35	3	1.69	3.99	0.000920	13.74	0.0126	0.8701
50	5.136	2	<100	35	3	1.69	3.99	0.000714	13.95	0.0100	0.6948
20	3.434	2	<100	35	3	1.69	2.67	0.000865	13.38	0.0116	0.9379
20	5.136	2	<100	35	3	1.69	3.99	0.001335	11.77	0.0157	0.9058
20	10.27	2	<100	35	3	1.69	7.98	0.001480	18.17	0.0269	0.9094
20	15.41	2	<100	35	3	1.69	11.98	0.001675	16.83	0.0282	0.9320
20	5.136	1	<100	35	3	0.85	3.99	0.001075	15.64	0.0168	0.7155
20	5.136	2	<100	35	3	1.69	3.99	0.001335	11.77	0.0157	0.9058
20	5.136	3	<100	35	3	2.54	3.99	0.001630	11.32	0.0185	0.7977
20	5.136	4	<100	35	3	3.38	3.99	0.001405	11.79	0.0166	0.8098
20	5.136	2	20-40	35	3	2.48	3.99	0.001325	4.42	0.0059	0.7403
20	5.136	2	40-60	35	3	2.33	3.99	0.001530	5.47	0.0084	0.8242
20	5.136	2	60-80	35	3	2.21	3.99	0.001285	7.10	0.0091	0.8527
20	5.136	2	80-100	35	3	2.09	3.99	0.000750	8.66	0.0065	0.7051
20	5.136	2	<100	35	3	1.69	3.99	0.001335	11.77	0.0157	0.9058
20	5.136	2	<100	25	3	1.69	3.99	0.001535	10.53	0.0162	0.8454
20	5.136	2	<100	35	3	1.69	3.99	0.001335	11.77	0.0157	0.9058
20	5.136	2	<100	45	3	1.69	3.99	0.001405	12.15	0.0171	0.9470
20	5.136	2	<100	35	1	1.69	3.99	0.001220	11.45	0.0140	0.9036
20	5.136	2	<100	35	2	1.69	3.99	0.001465	10.84	0.0159	0.9238
20	5.136	2	<100	35	3	1.69	3.99	0.001335	11.77	0.0157	0.9058
20	5.136	2	<100	35	4	1.69	3.99	0.001615	8.26	0.0133	0.9192
20	5.136	2	<100	35	5	1.69	3.99	0.001445	7.68	0.0111	0.9399
20	5.136	2	<100	35	6	1.69	3.99	0.001425	7.53	0.0107	0.9018
20	5.136	2	<100	35	7	1.69	3.99	0.001550	5.70	0.0088	0.8135
20	5.136	2	<100	35	8	1.69	3.99	0.001255	4.88	0.0061	0.6688
20	5.136	2	<100	35	9	1.69	3.99	0.000445	4.99	0.0022	0.9808
20	5.136	2	<100	35	10	1.69	3.99	0.000590	4.83	0.0029	0.9433

APPENDIX C

Effect of influent flow rate on the Yoon-Nelson model parameters τ, t_1 and t_2.

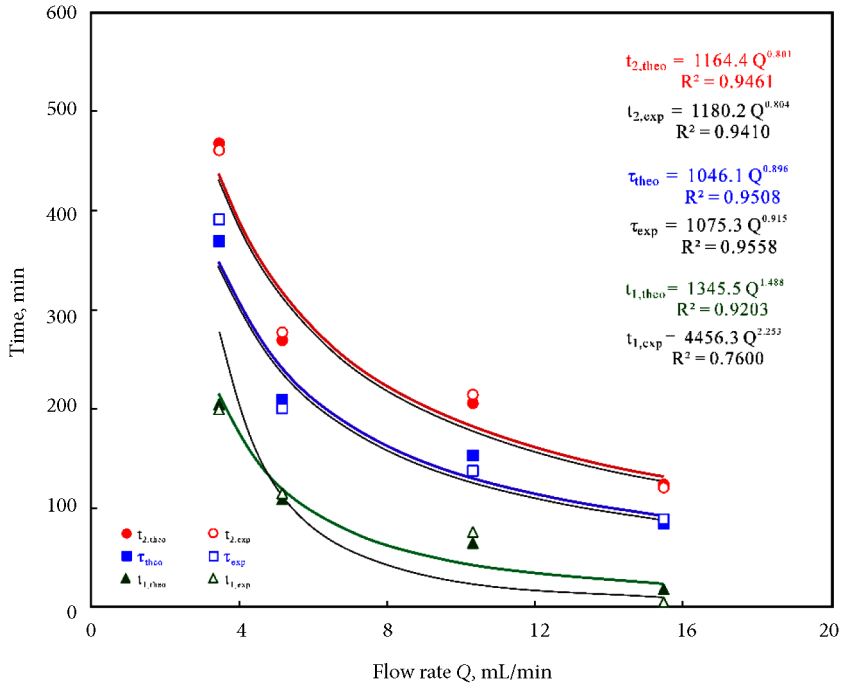

APPENDIX D
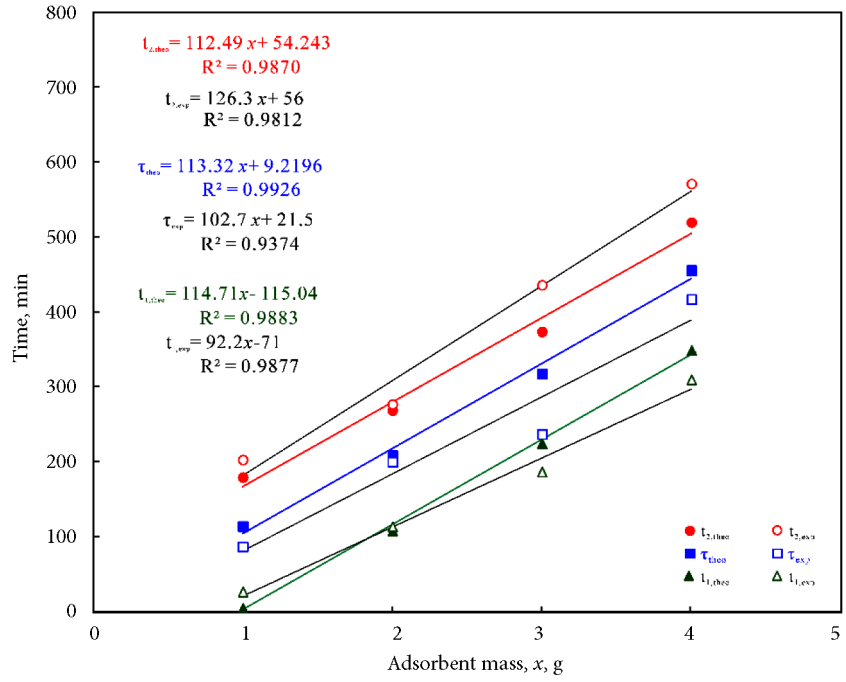
Effect of adsorbent mass on the Yoon-Nelson model parameters τ, t_1 and t_2.